NOAA Technical Memorandum ERL NHRL-93

U.S. DEPARTMENT OF COMMERCE
NATIONAL OCEANIC AND ATMOSPHERIC ADMINISTRATION
Environmental Research Laboratories

Horizontal Asymmetries in a Numerical Model of a Hurricane

JAMES W. TROUT

RICHARD A. ANTHES

National
Hurricane
Research
Laboratory
CORAL GABLES,
FLORIDA
November 1971

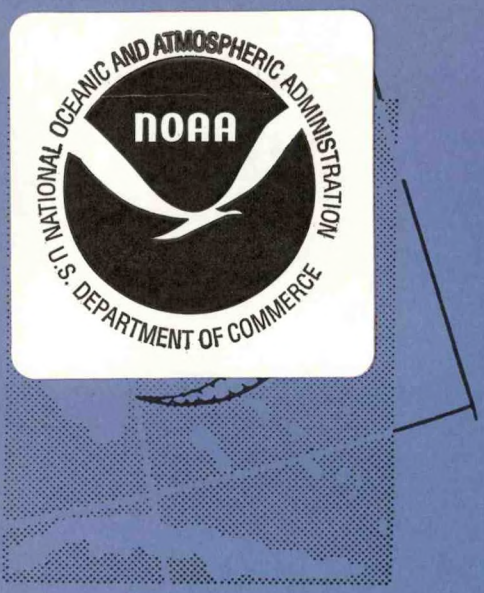

NATIONAL OCEANIC AND ATMOSPHERIC ADMINISTRATION

ENVIRONMENTAL RESEARCH LABORATORIES

NATIONAL HURRICANE RESEARCH LABORATORY TECHNICAL MEMORANDA

Reports by units of the NOAA Environmental Research Laboratories, contractors, and cooperators working on the hurricane problem are preprinted in this series to facilitate immediate distribution of the information among the workers and other interested units. As the limited reproduction and distribution in this form do not constitute formal scientific publication, reference to a paper in the series should identify it as a preprinted report.

Other reports in this series have been prepared by the National Hurricane Research Project of the U.S. Weather Bureau, by the National Hurricane Research Laboratory, as a part of the Weather Bureau Technical Note Series, and as NHRL Technical Memoranda, a subseries of the Institute of Environmental Research Technical Memoranda series.

Beginning with No. 81, they are identified as NHRL Technical Memoranda, a subseries of the ESSA Research Laboratories (ERL). Beginning with No. 90, they are identified as ERL NHRL Technical Memoranda, a subseries of the NOAA Environmental Research Laboratories (ERL).

The reports are available, at a cost of $3.00 per hard copy (microfiche 95 cents), from the National Technical Information Service, Operations Division, Springfield, Virginia 22151.

U.S. DEPARTMENT OF COMMERCE
National Oceanic and Atmospheric Administration
Environmental Research Laboratories

NOAA Technical Memorandum ERL NHRL-93

HORIZONTAL ASYMMETRIES IN A NUMERICAL MODEL OF A HURRICANE

James W. Trout
Richard A. Anthes

National Hurricane Research Laboratory
Coral Gables, Florida
November 1971

TABLE OF CONTENTS

HORIZONTAL ASYMMETRIES IN A NUMERICAL MODEL OF A HURRICANE

James W. Trout and Richard A. Anthes

Statistical techniques are employed to investigate the development and structure of horizontal asymmetries in the numerical model of a hurricane developed by Anthes et al. (1971a). Strong asymmetries in the momentum and temperature fields develop in the outflow layer at approximately 120 hours. Weaker asymmetries also develop in the inflow layer at this time. Harmonic analyses are used to determine the predominant scale of asymmetries. Detailed spatial analyses are carried out for the momentum and temperature fields in the mature asymmetric stage of the model. The analyses are compared to observational data compiled by Black and Anthes (1971). The results show that the model reproduces many observed features of a three-dimensional tropical cyclone.

1. INTRODUCTION

Recent experiments conducted with an asymmetric hurricane model (Anthes et al., 1971a) dramatically illustrate certain asymmetric properties of the horizontal and vertical motion fields. Examples of these are horizontal eddies in the upper tropospheric outflow layer, rainbands, and meandering of the hurricane eye. Two distinct stages are observed in a typical experiment. During the early stages, the storm circulation is quite symmetric about the vertical axis of rotation. In the second stage, the storm acquires marked asymmetric characteristics in the outflow layer, and the vertical motion patterns form spiral bands which resemble hurricane rainbands.

The purpose of this paper is to report the quantitative investigation of the nature and importance of the asymmetric character of the model storm. Various statistical measures are employed to show the

time-dependent development and locations of the asymmetries. Harmonic analysis of the radial and tangential wind components determines the predominant scale of the asymmetries. Computations of fluxes of angular momentum and absolute vorticity show the importance of asymmetries as horizontal transport mechanisms. The asymmetries in the model outflow layer are compared with the asymmetric features of real storms (Black and Anthes, 1971).

2. SUMMARY OF THE MODEL

The equations are written in σ-coordinates (Phillips, 1957) on an f-plane. The equations of motion and the continuity, thermodynamic, and hydrostatic equations are identical to those utilized by Smagorinsky et al. (1965) for general circulation studies. The basic equations are given in Anthes et al. (1971a). The vertical structure of the model consists of an upper layer and a lower layer of equal pressure depth and a thinner Ekman boundary layer. The information levels for the dynamic and thermodynamic variables are staggered according to the method used by Kurihara and Holloway (1967).

For computational economy, the horizontal mesh has been limited to a square grid with a uniform spacing of 30 km. The lateral boundary points approximate a circle, and all points are contained between radii of 435 and 450 km. The thermodynamic grid points are staggered from the velocity component grid points on the σ-surfaces. A comprehensive summary of the mathematical details is given elsewhere (Anthes, 1972) and need not be repeated here.

The Matsuno (1966) simulated forward-backward scheme is utilized in the model for the time integration scheme. The Matsuno scheme has the property of dampening the very high temporal frequencies associated with internal and external gravity waves. The lateral boundary conditions consist of a steady-state pressure and temperature on the boundary and a variable momentum based on extrapolation outward from the interior of the domain. The cumulus scale convective processes are parameterized similarly to the version of Rosenthal's (1970b) symmetric model. The current model also contains an explicit water vapor cycle. For further details refer to Anthes (1972). The initial conditions consist of an axisymmetric vortex in gradient balance. The minimum pressure is 1011 mb, and the environmental pressure on the lateral boundary is 1015 mb, yielding a maximum gradient wind of 18 m sec^{-1} at a radius of 240 km. With these initial conditions and utilizing a time step of 45 seconds, the experiment has been executed for 192 hours.

With symmetric initial and boundary conditions, the solutions to the differential equations must remain symmetric for all time. However, truncation and roundoff errors in the finite difference equations, as well as the lack of complete circular symmetry in boundary conditions, produce extremely weak asymmetries after the first time step. Although objections might be raised concerning the desirability of allowing the initial asymmetries to be generated by truncation, later experiments in which asymmetries were deliberately introduced in a random fashion yield essentially the same results during the asymmetric stage (Anthes, 1972).

Thus, it appears that the actual source of the initial asymmetries is unimportant in the mature asymmetric stage.

3. COMPUTATIONAL PROCEDURE

During the asymmetric stage an interesting anticyclonic looping of the eye is observed. This looping appears to be related to the asymmetric outflow and is discussed by Anthes (1972). The center of the grid is depicted as zero (fig. 1), with north-south, east-west deviations from the center plotted in kilometers.

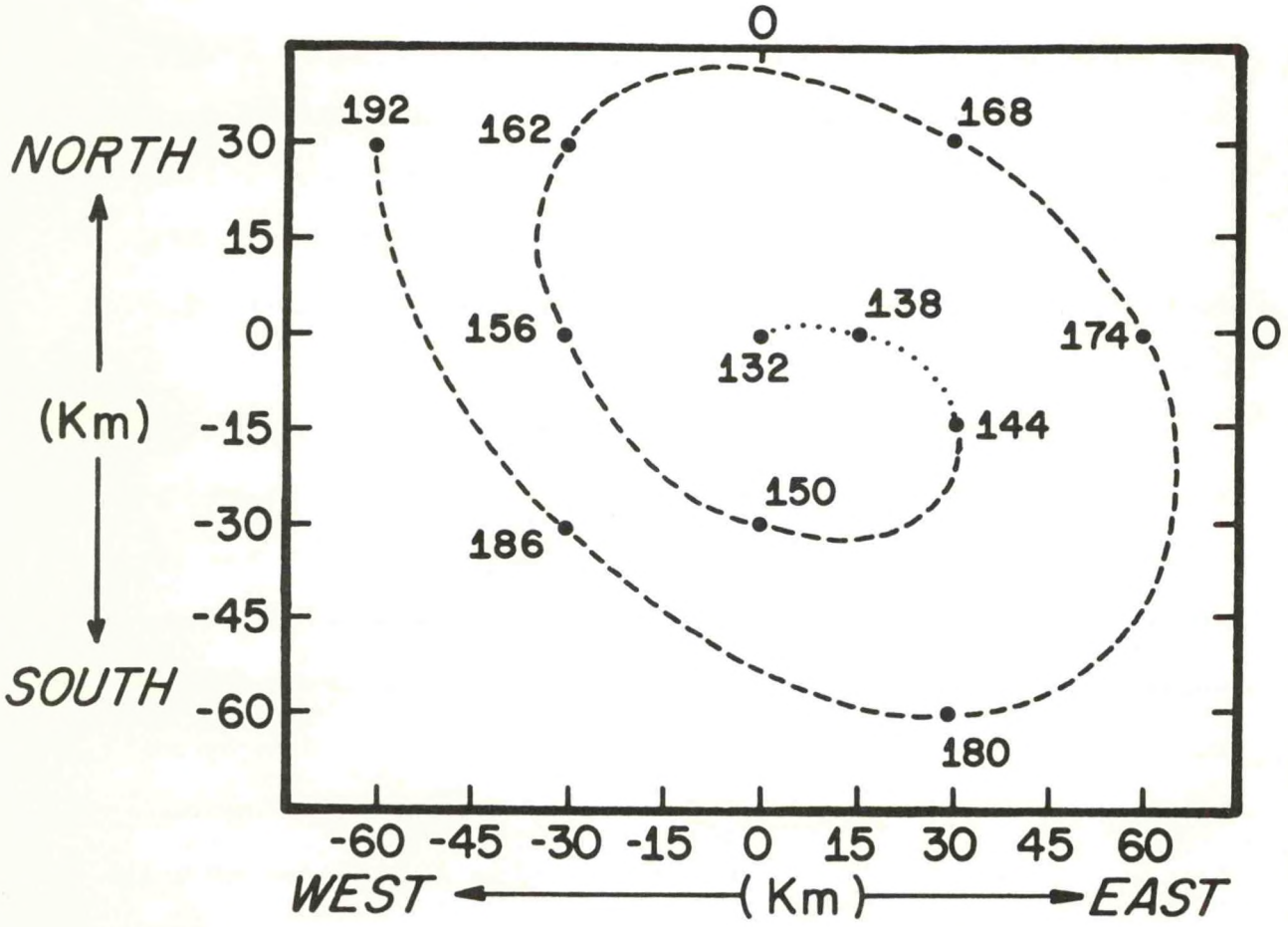

Figure 1: Model vortex motion. Positions are labeled in hours.

3.1 The Polar Grid

The computation of circular averages and mean and eddy fluxes of vorticity and momentum requires interpolation from the cartesian grid system to a polar grid system whose origin is coincident with the looping vortex center. The rectangular (u) and (v) wind components are converted into tangential (V_λ) and radial (V_r) wind components by use of:

$$V_\lambda = (vX - uY)/R \tag{1}$$

and

$$V_r = (uX - vY)/R \tag{2}$$

where X and Y are the distances along the x and y axis between the vortex center and a given grid point;

and $$R = (X^2 + Y^2)^{\frac{1}{2}}. \tag{3}$$

The cartesian arrays are interpolated to a polar coordinate grid consisting of 15 radial increments of 30 km (r = 15, 45, 75....) and 16 azimuthal increments of 22.5 degrees. The calculation extends to a radius of 435 km when the storm center is located on the center of the cartesian grid. When the storm center is located away from the grid center, the maximum radius of the polar grid is reduced.

3.2 Interpolation Schemes to the Polar Grid

The accuracy of two interpolation formulae is tested. The first of these is a bilinear interpolation formula:

$$\overline{S}^1 = S_{I,J} + h[S_{I,J+1} - S_{I,J}] + K[(S_{I+1,J} - S_{I,J})\ (1-h) + (S_{I+1,J+1} - S_{I,J+1})j]. \tag{4}$$

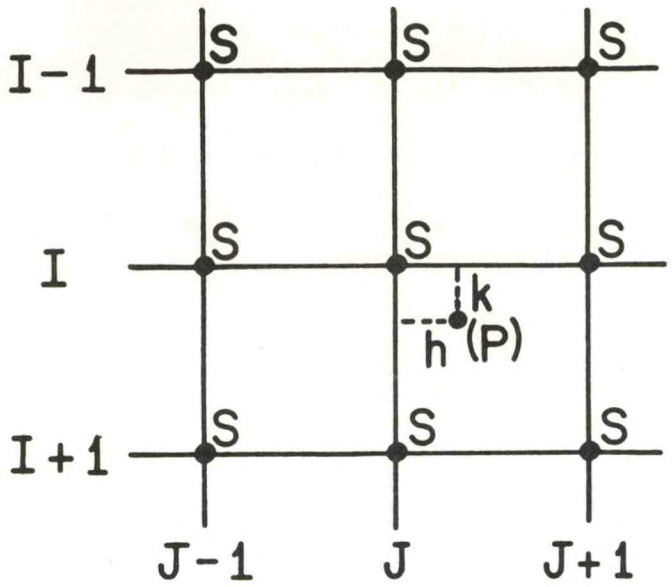

Figure 2: Interpolation to polar grid point (P).

Here the interpolated value of S, at the location of the polar point (fig. 2), is denoted by P. In (4), (I,J) is the grid point (row, column) index in the usual matrix sense; h and K are the coordinate distances from point P to grid point (I,J). Satisfactory results are obtainable with (4) at large radii. However, at smaller radii the curvature in the variables associated with the hurricane vortex is too extreme for linear interpolation. The second method is a nine point interpolation function. The formula is a finite difference form of the truncated Taylor's expansion of a function of two independent variables.

$$\overline{S}^2 = S_{I,J} + .5h(S_{I,J+1}-S_{I,J-1}) + .5K(S_{I-1,J}-S_{I+1,J})$$

$$+ .5h^2(S_{I,J+1}+S_{I,J-1}-2S_{I,J}) + .5K^2(S_{I-1,J}+S_{I+1,J}-2S_{I,J})$$

$$+ .25hK(S_{I-1,J+1}-S_{I-1,J-1}-S_{I+1,J+1}+S_{I+1,J-1}). \qquad (5)$$

For all interpolations the base point (I,J) is selected so that h and K are not greater than one-half a grid increment.

Both interpolation formulae are applied to the function,

$$f(r) = (r+15)/30 \qquad (r \text{ in km}). \tag{6}$$

With the vortex center coincident with the grid center, (6) yields integer values increasing from 1 at r = 15 km to 15 at r = 435 km at all azimuth angles. Table 1 shows circular averages, for the first five radii, computed from data obtained by use of (4) and (5).

Table 1: Circular Averages Computed from Interpolation Scheme (4) and (5)

Radius (km)	Bilinear Interpolation Eqn. (4)	9-Point Interpolation Eqn. (5)
15	1.2071	1.0969
45	2.0529	2.0137
75	3.0447	2.9920
90	4.0211	4.0022
105	5.0230	5.0008

Table 1 clearly shows the superiority of the 9-Point Interpolation formula at small radii. Hence, interpolation formula (5) is utilized throughout this paper.

4. THE ASYMMETRIC STAGE

Notable asymmetries of the cyclone circulation include large horizontal eddies in the upper tropospheric outflow region. Figure 3 shows the trajectories of 10 particles which are released in the lower levels of the cyclone and provides a qualitative view of the asymmetric circulation over the life cycle of a typical experiment. The trajectories are

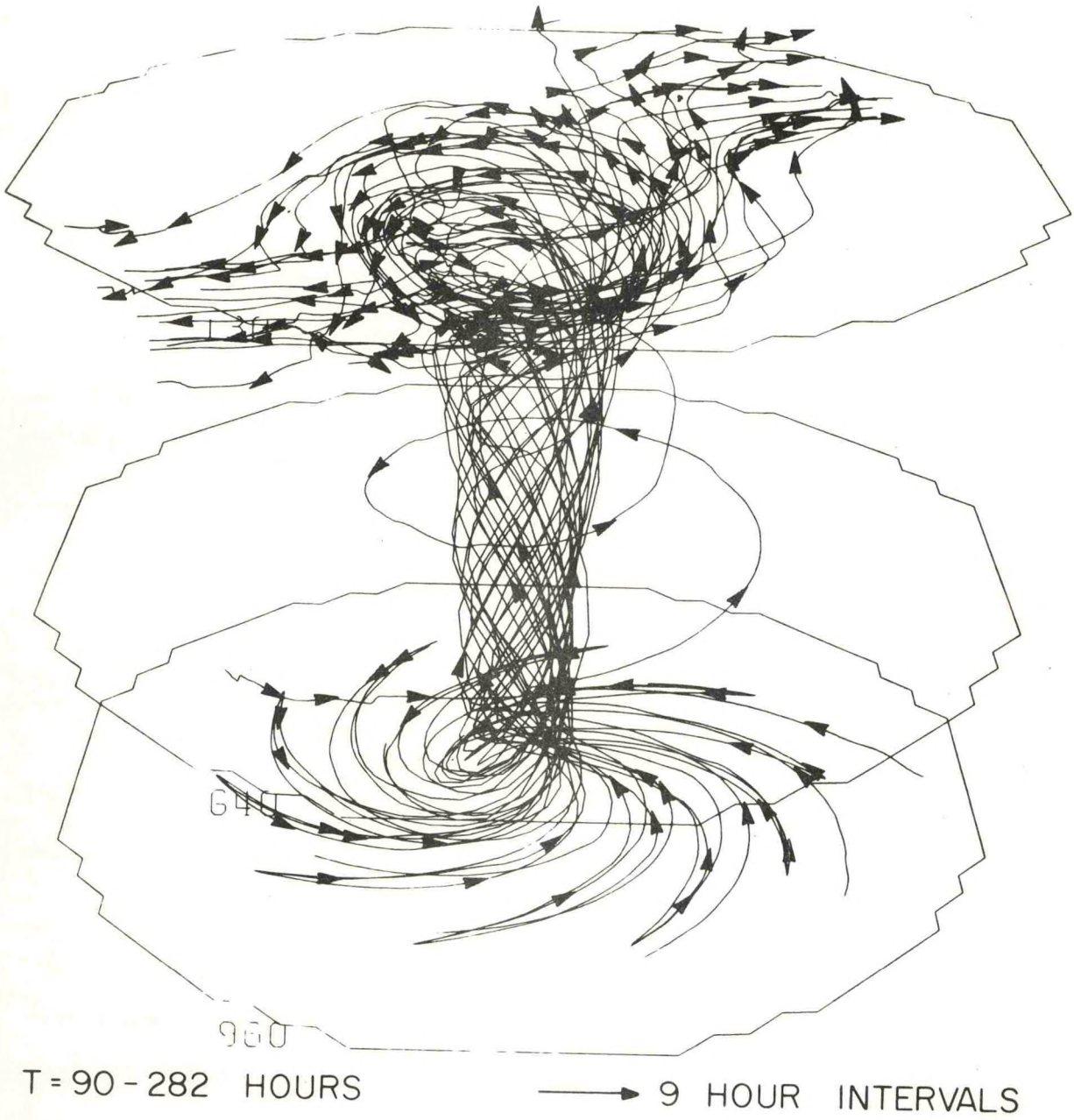

Figure 3: Ten trajectories of parcels released in the boundary layer over an 8-day period.

computed over an 8-day period from the forecast velocity components. For additional illustrations and computational procedure refer to Anthes et al. (1971c). The figure greatly exaggerates the vertical dimension of the storm but clearly illustrates the asymmetric outflow characteristics. Particles, upon reaching the upper levels of the model, are carried outward from the vortex center, mainly in the northeast and southwest quadrants. This should be contrasted to the nearly symmetric inflow depicted in the lower layers. The preferred quadrants of outflow reflect the asymmetric circulation around upper level horizontal eddies that are present during the 8-day period.

4.1 Time Variations of Azimuthal Standard Deviations

The principal measure of asymmetry employed here is the standard deviations (SD) from the azimuthal averages of momentum and temperature. Figure 4 and figure 5 are plots of SD versus time for the radial winds, tangential winds and temperature at selected radii in the inflow and outflow layers.

Large SD are computed at very small radii (not plotted), where the interpolation error due to the relatively few cartesian grid point values is the greatest. However, the asymmetries are relatively small compared to the azimuthal means. The inflow asymmetries diminish rapidly with increasing radius. The outflow asymmetries, on the other hand, appear to be greatest near the 165 km radius (fig. 4). The ratio of the standard deviation to the mean at all radii is larger in the outflow layer.

Three distinct development phases of the model can be defined from the time variation of the SD. First, there is an "organizational phase,"

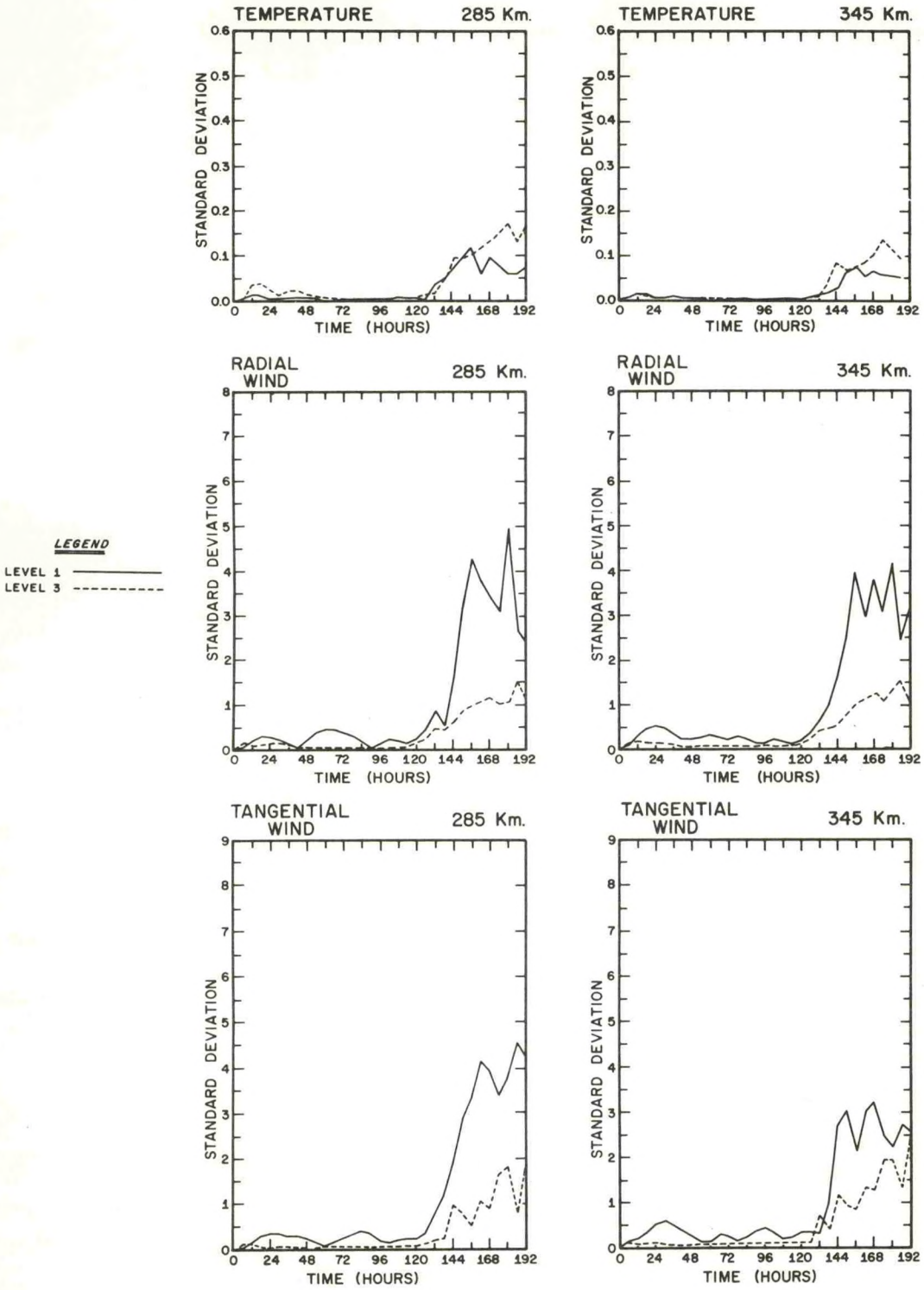

Figure 4: Time variations of the standard deviations for temperatures, radial winds, and tangential winds at inner radii.

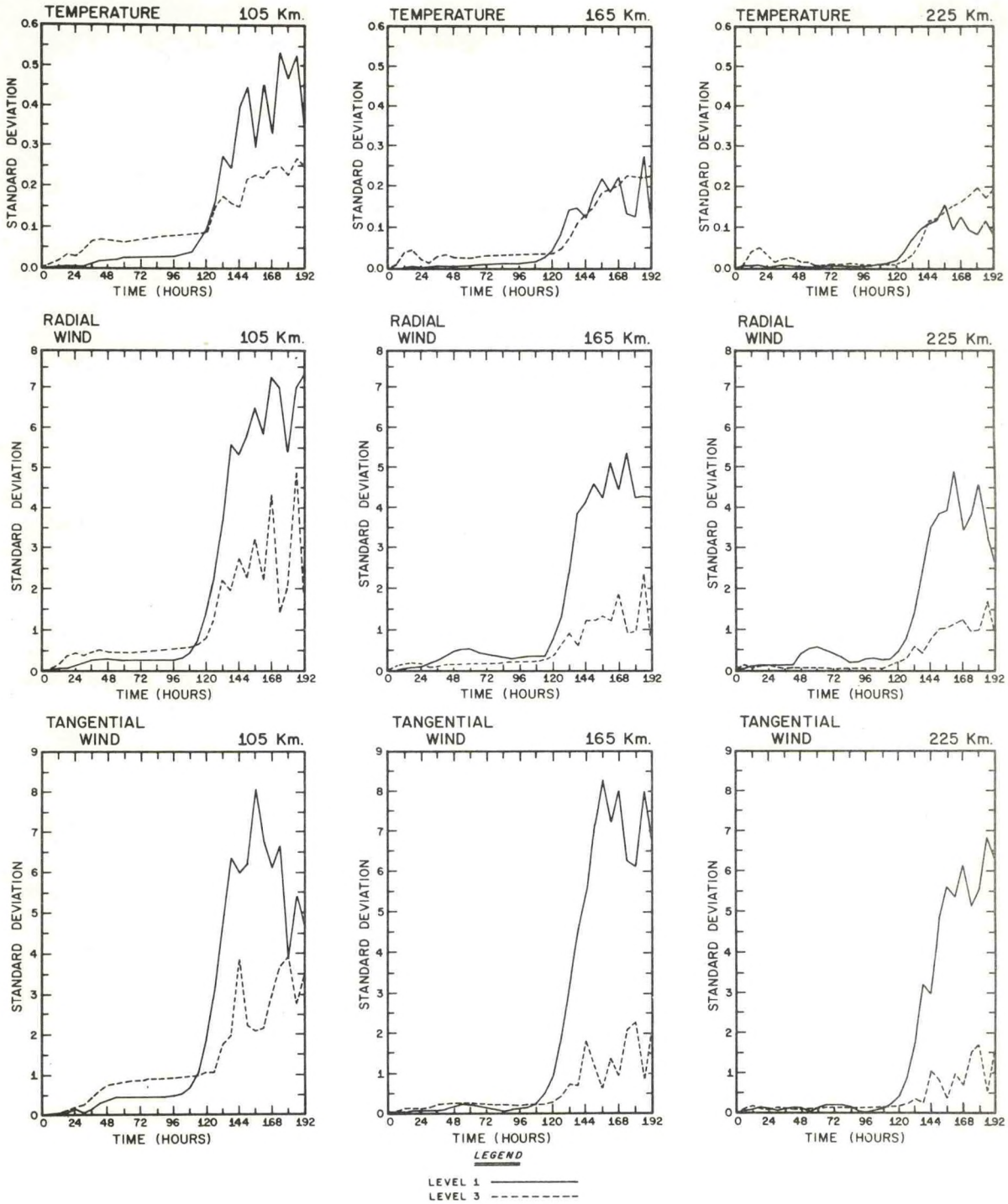

Figure 5: Time variations of the standard deviations for temperatures, radial winds, and tangential winds at outer radii.

exhibited initially by the lack of asymmetries. Standard deviations of 0.5 m sec^{-1} or less are computed for both the radial and tangential winds during this phase. Increasing deviations first appear in the inflow layer and this is closely followed by the development of small asymmetries in the outflow layer. A period (symmetric phase) in which the SD's are small and relatively steady follows. Finally, an asymmetric phase begins at approximately 120 hours. This is characterized by the development of large scale asymmetries in the outflow layer and spiral bands of convection in the lower layer. At small radii, the SD of the tangential winds increases to 8 m sec^{-1} in the outflow layer. The asymmetries in the outflow layer radial wind field also experience rapid growth, but the magnitude of the SD is somewhat smaller than that of the tangential winds. The magnitude of the asymmetries of the two components is comparable in the inflow layer as are the circular means.

At the larger radii, both the inflow and outflow asymmetries decrease with increasing radius (figs. 4 and 5). However, at a radius of 350 km from the vortex center, the asymmetries are still well defined and contain SD approximately equal to the magnitude of the mean radial and tangential flow. The lateral boundary conditions require the boundary velocity components to vanish at inflow points, and thus contribute to decreased SD's at large radii in the inflow layer.

The plots of temperature SD versus time also distinctly illustrate the three phases of the development of the model. However, the temperature field is much more symmetric than the momentum field, as indicated by the small standard deviations of temperature. The decrease of SD with

increasing radius is due to the boundary conditions of a steady symmetric temperature.

4.2 Harmonic Analysis of the Momentum and Temperature Fields

The previous section established the rapid development of asymmetries at model time equal to 120 hours. In this section harmonic analysis establishes the predominant scale of the asymmetries for both the inflow and outflow levels. Figures 6, 7, and 8 show the time variation of the scale of the percent variance accounted for by harmonic 1, 2, 3, 4, and 8 at a typical inner (45 km) and outer (285 km) radius of the vortex.

An important feature revealed by the harmonic analysis is the predominance of wave numbers 4 and 8 during the organizational and symmetric stages of the vortex development. The grid boundary is an 8-sided figure comprised of 4 regular sides and 4 irregular sides. Wave number 8 is, therefore, probably a manifestation of the octagon shaped boundary of the grid. Wave number 4 is apparently a manifestation of the 4 irregular corners of the grid. Both wave patterns are also affected by errors associated with the numerical differencing scheme, especially in corner regions of the grid where the lateral boundary conditions may cause different truncation errors. Recent investigations by Koss (1971) show that the numerical differencing utilized in an asymmetric vortex model can also induce error patterns that persist with time in the form of wave number 4. Caution must be exercised in interpreting figures 6, 7, and 8. During the early stages of the experiment, the percent of variance contained by wave number 4 is very high (70% to 95%); however, the total

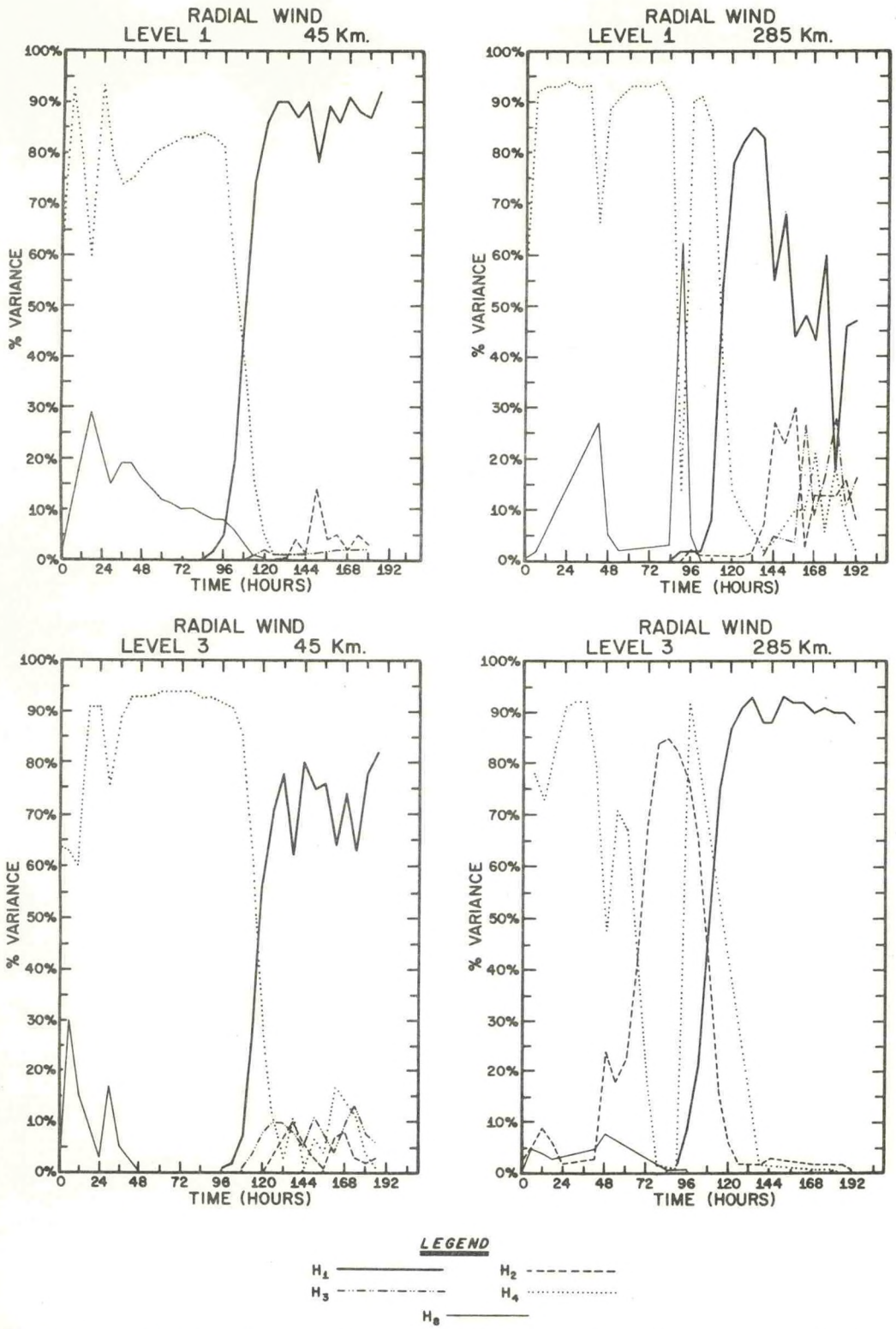

Figure 6: Harmonic analysis of the model outflow layer and inflow layer radial wind component. Wave numbers 1, 2, 3, 4, and 8 are illustrated at an inner and outer radius.

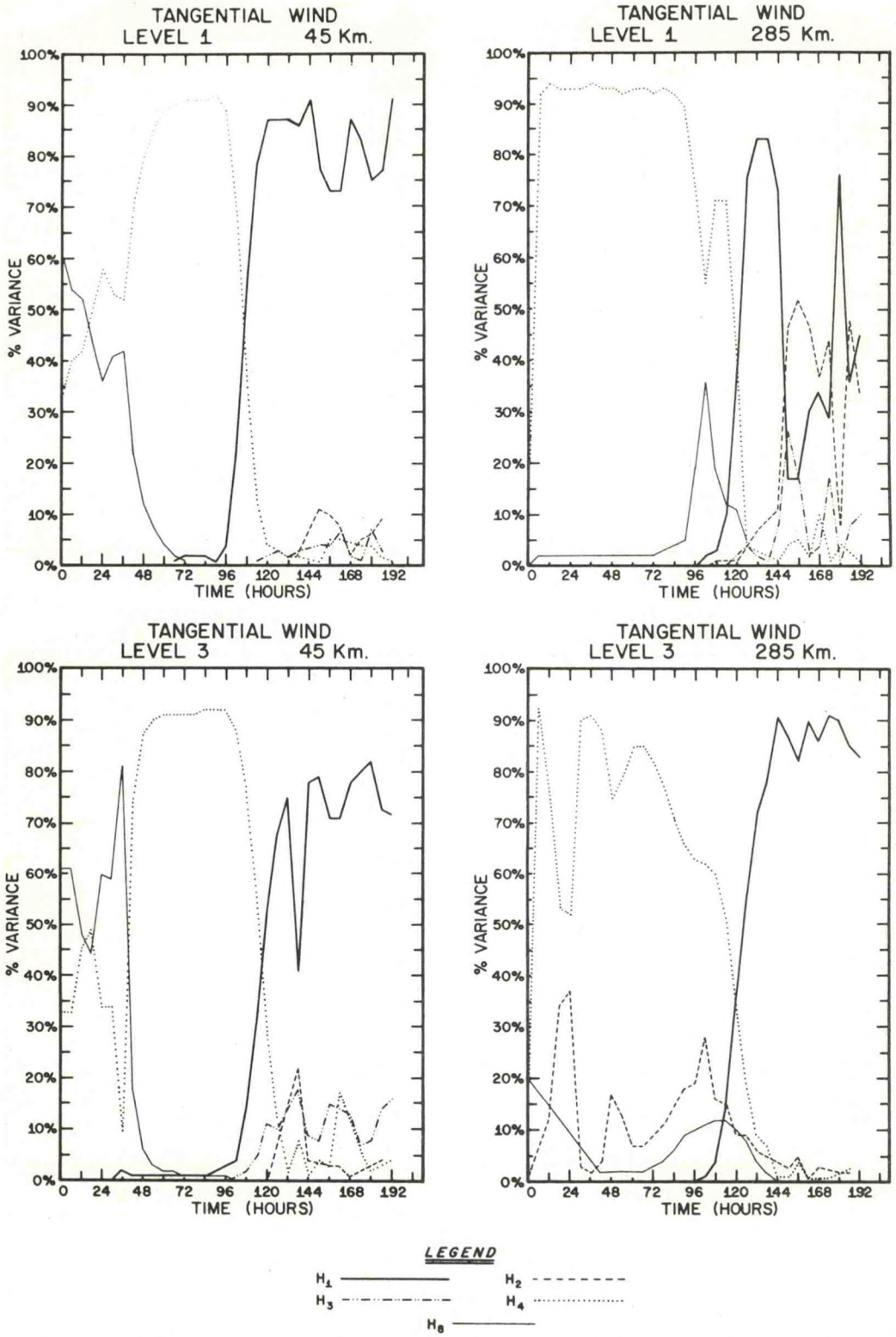

Figure 7: Harmonic analysis of the model outflow layer and inflow layer tangential wind component. Wave numbers 1, 2, 3, 4, and 8 are illustrated at an inner and outer radius.

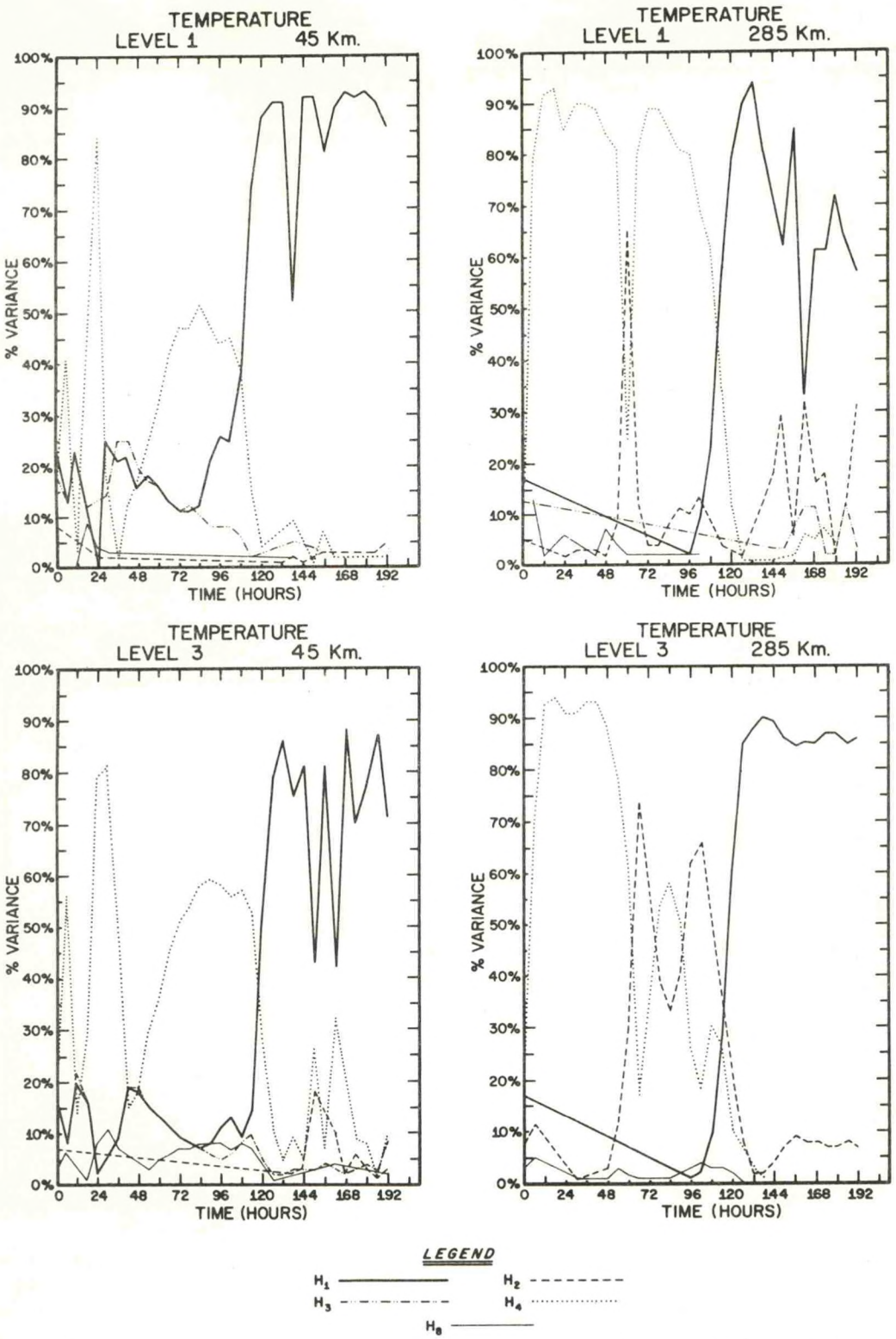

Figure 8: Harmonic analysis of the model outlfow layer and inflow layer temperatures. Wave numbers 1, 2, 3, 4, and 8 are illustrated at an inner and outer radius.

variance is very small. The SD of the tangential wind, for example, is only about 0.5 m sec^{-1} contrasted with the mean flow of about 10 m sec in the outflow and 30 m sec^{-1} in the inflow layers.

The boundary induced wave numbers 4 and 8 are rapidly obscured by the presumably meteorological waves, 1, 2 and 3 with the onset of the asymmetric stages of the model. Figures 6, 7, and 8 all show the wave 4 trace and wave 1 trace intersecting at a time slightly less than 120 hours. Thereafter, the predominant wave is clearly wave 1 for both inflow and outflow layers. Recent results (Anthes, 1972) show the growth of asymmetries in the outflow layer to be a result of barotropic instability in which the energy source of the eddies is the kinetic energy of the mean flow. The temperature harmonic analysis shows essentially the same behavior as the momentum analysis, with wave number 1 becoming predominant during the asymmetric stage. In summary it should be reemphasized that the total variance in the inflow layer is small and that the temperature variance is small at both levels.

5. EDDY FLOW RELATED TO THE MATURE VORTEX

This section presents a detailed analysis of the eddy flow in both the inflow and outflow levels during the mature stage of the vortex (174 hours). Figures 9 and 10 are the streamline and isotach analysis for the outflow and inflow levels, respectively. The asymmetric circulation in the outflow layer, the displacement of the vortex center from the grid center, and the relative symmetry of the inflow level, discussed earlier, are again illustrated by these figures. The isotach analysis shows that

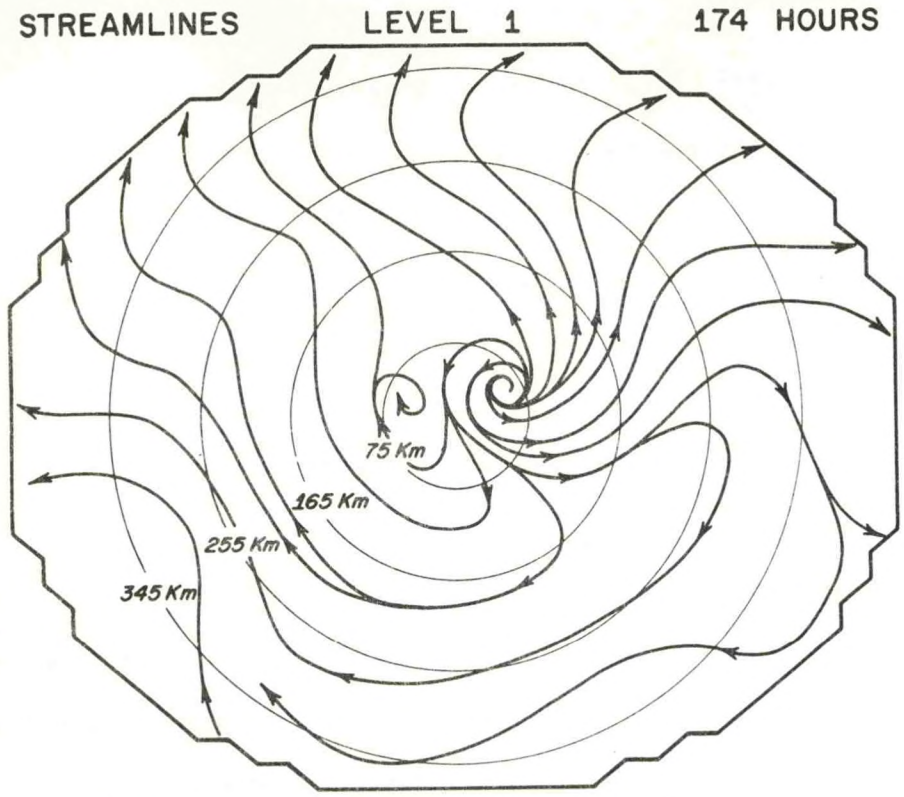

Figure 9A: Streamlines - Level 1 - 174 hours.

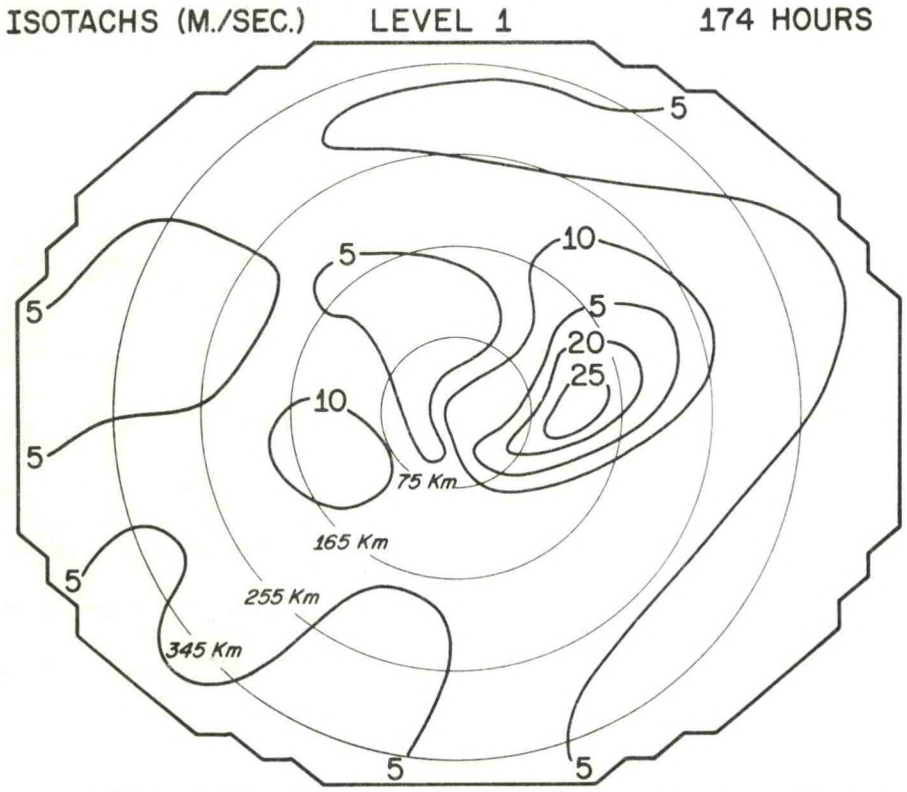

Figure 9B: Isotachs (m./sec.) - Level 1 - 174 hours.

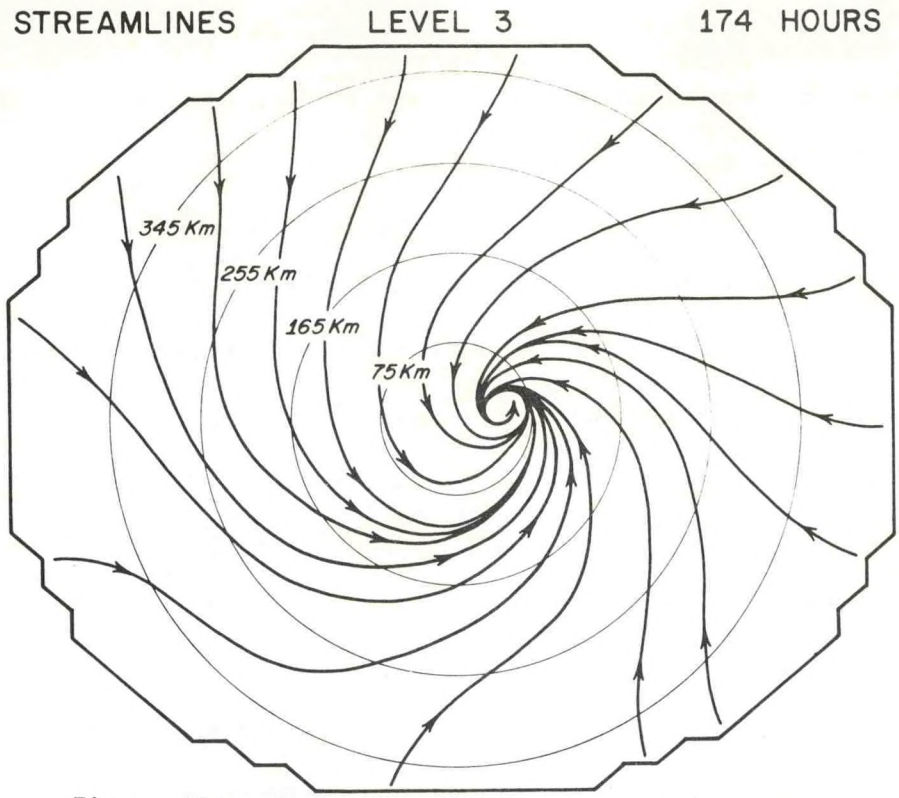

Figure 10A: Streamlines - Level 3 - 174 hours.

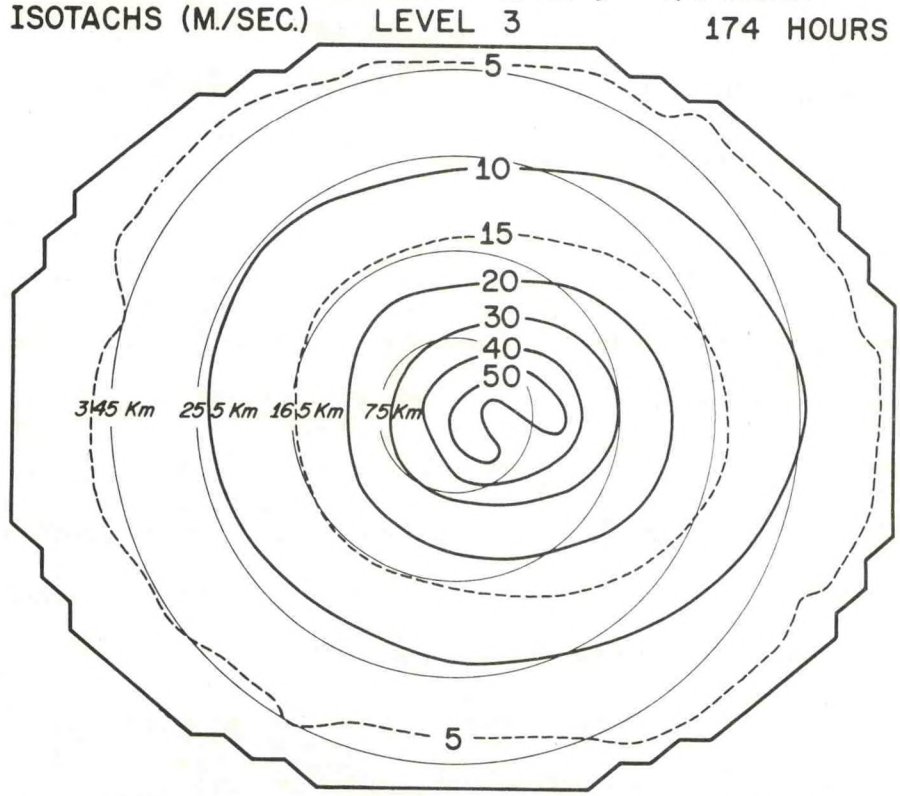

Figure 10B: Isotachs (m./sec.) - Level 3 - 174 hours.

at least one or two maxima and minima can be located about the storm's center in the outflow layer.

5.1 Asymmetries in the Outflow Layer

Figure 11 shows the azimuthal means and SD for the upper level wind components at 174 hours. The radial component is characterized by outflow at all radii, with a maximum value of 7 m sec^{-1} at 75 km. The outflow velocities decrease with increasing radii to a value of 2 m sec^{-1} at 435 km, the edge of the domain. The tangential component is characterized by a strong band of cyclonic winds near the center, with a maximum of 14 m sec^{-1} at 45 km. The mean tangential winds become anticyclonic at a radius of 135 km and remain anticyclonic with increasing radii.

Black and Anthes (1971) used cirrus band motions, radiosonde winds, and limited aircraft data to construct similar figures for six individual Atlantic storms. They also presented data from Miller's (1958) mean Atlantic storm and Izawa's (1964) mean Pacific storm. However, their calculations begin at approximately 105 km from the center and extend well beyond 435 km. Two limitations exist in comparing the real storm data to the model storm data. First, the isolated nature of the vortex implies that the asymmetries and the mean flow diminish as the boundary is approached. In contrast, in the real atmosphere, the flow patterns at large radii interact with other atmospheric systems which produce additional asymmetries. Second, near the center of the storms, Black and Anthes' data are compiled utilizing a coarse grid of 111 km as compared to the 30 km model grid. With these limitations in mind, a comparison between the model figures and the actual storm data shows:

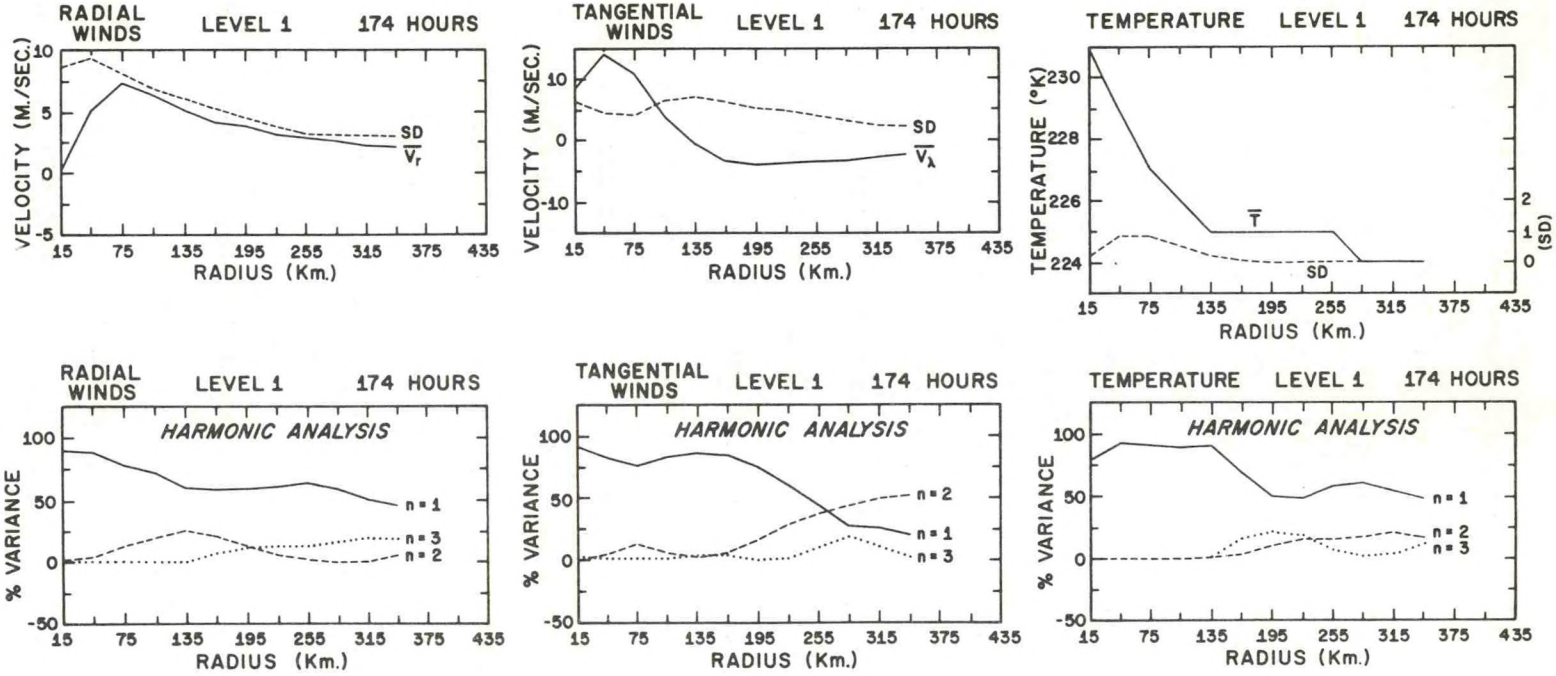

Figure 11: Standard deviations (SD), azimuthal means (-), and percent variance accounted for by wave numbers 1-4 for the mature outflow layer.

1. There is favorable agreement between the magnitude of the model mean radial wind component (V_r) compared with the six Atlantic storms. However, the magnitude of V_r is larger than either the Pacific or Atlantic mean profiles. Defining symmetry as a high ratio of the mean to the SD, the following comparisons of real and model outflow can be made:

(a) The SD approaches the magnitude of the mean radial wind in both the model and actual storm data.

(b) The magnitude of $\overline{V}_r$ falls within the range of the magnitude of the real storm's radial winds.

(c) At large radii, the real storm tends to be more asymmetric than the model storm because the latter diminishes in intensity with increasing radius and the former merges with other large scale circulations.

(d) The magnitude of the asymmetries compares favorably with that of the mean Atlantic and Pacific storm's radial winds.

The harmonic analyses reveal the dominance of wave number 1 for both the model and the actual storm outflow. The percent of variance accounted for by the higher order wave numbers at increasing radii indicates the presence of more than one eddy in the outflow layer far from the model vortex center.

2. There is also favorable agreement between the magnitude of the model mean tangential wind component ($\overline{V}_\lambda$) compared with the actual storm data, although again the model storm circulation is somewhat smaller in radial extent than the real storm circulation. Specifically, the model storm and the real storm show:

(a) a low ratio of the SD to the mean at inner radii, indicating symmetry;

(b) a higher ratio of the SD to the mean at the outer radii, indicating asymmetry;

(c) standard deviations for both tangential and radial wind components of about the same order of magnitude.

The harmonic analysis again shows a predominance of wave number 1 associated with the $\overline{V}_{\lambda}$. Higher wave numbers appear at radii greater than 200 km and account for a larger percent of the variance than the higher wave numbers associated with V_r.

Figure 12 shows the temperature departures from the mean tropical sounding (Herbert and Jordan, 1959) for both the inflow and outflow levels. The maximum departure of 7 degrees occurs to the east of the vortex center with smaller departures occurring to the west of the center. The SD are small (less than 1°C) at all radii and approach zero with increasing radius, reflecting the steady state, uniform boundary conditions imposed on the temperature fields. The symmetry ratio of the mean to the SD is large, indicating that the temperature is nearly symmetric. The harmonic analysis shows a large percentage of the variance to be contained in harmonic one, with higher harmonics becoming more important at large radii.

In summary, the model outflow momentum components are quite asymmetric, in agreement with the outflow asymmetries of the wind fields found in real storms. The temperature field is considerably more symmetric than the corresponding wind fields.

TEMPERATURE DEPARTURES
174 HOURS

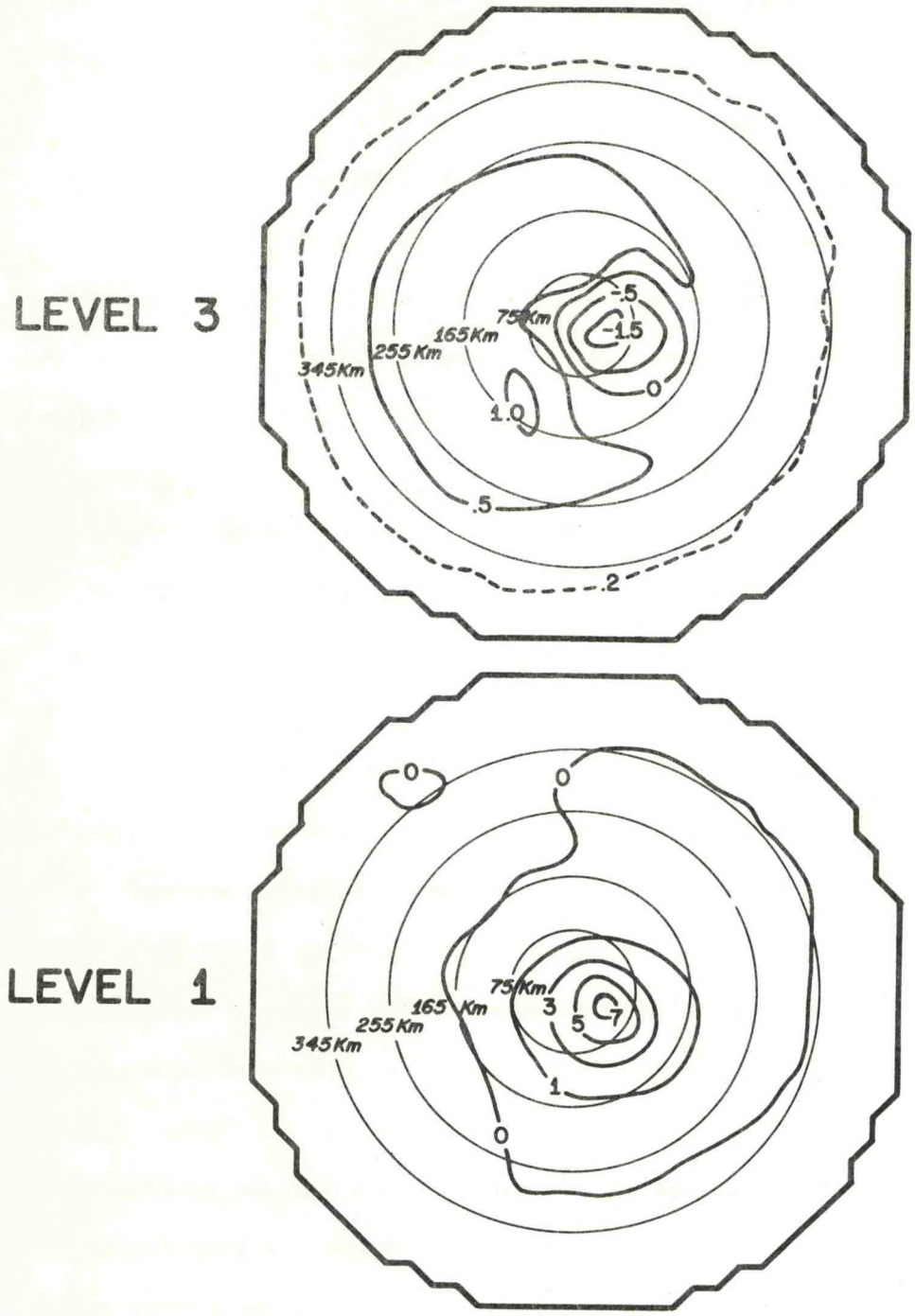

Figure 12: Temperature departures - 174 hours.

5.2 Asymmetries in the Inflow Layer

Figure 13 exhibits the inflow level mean radial profiles and harmonic analysis for the model momentum and temperature fields at time equal to 174 hours. Real storm data for a direct comparison are difficult to obtain since most low-level studies have been performed at elevations considerably above the boundary layer.

The radial wind component is characterized by an inflow maximum of 28 m sec^{-1} occurring at a radius of 75 km (same radius as the maximum outflow component). The inflow maximum rapidly diminishes to a value of approximately 1 m sec^{-1} at R_{max} (435 km). The small ratio of the SD to the mean indicates some minor asymmetry at the outer radii. These features are within observable limits, but they are difficult to substantiate. This ratio is much smaller in the inflow layer than in the outflow layer, indicating a closer approximation to axial symmetry in the low levels.

The radial wind harmonic analysis shows that wave number 1 explains approximately 80-90 percent of the variance from 135 km outward. A possible verification of the dominance of wave 1 in the boundary level could be the track of low-level actual storm radar echoes as reported by Black (1971). By tracking and plotting the variations of echo velocities about an actual hurricane, Black found patterns which reproduced a nearly sinusoidal wave--hence, wave number 1.

Inward from 135 km, wave number 4 is large in the model storm. Additional data (not presented) show wave number 4 to be a persistent feature of the model during its life history before and after 174 hours.

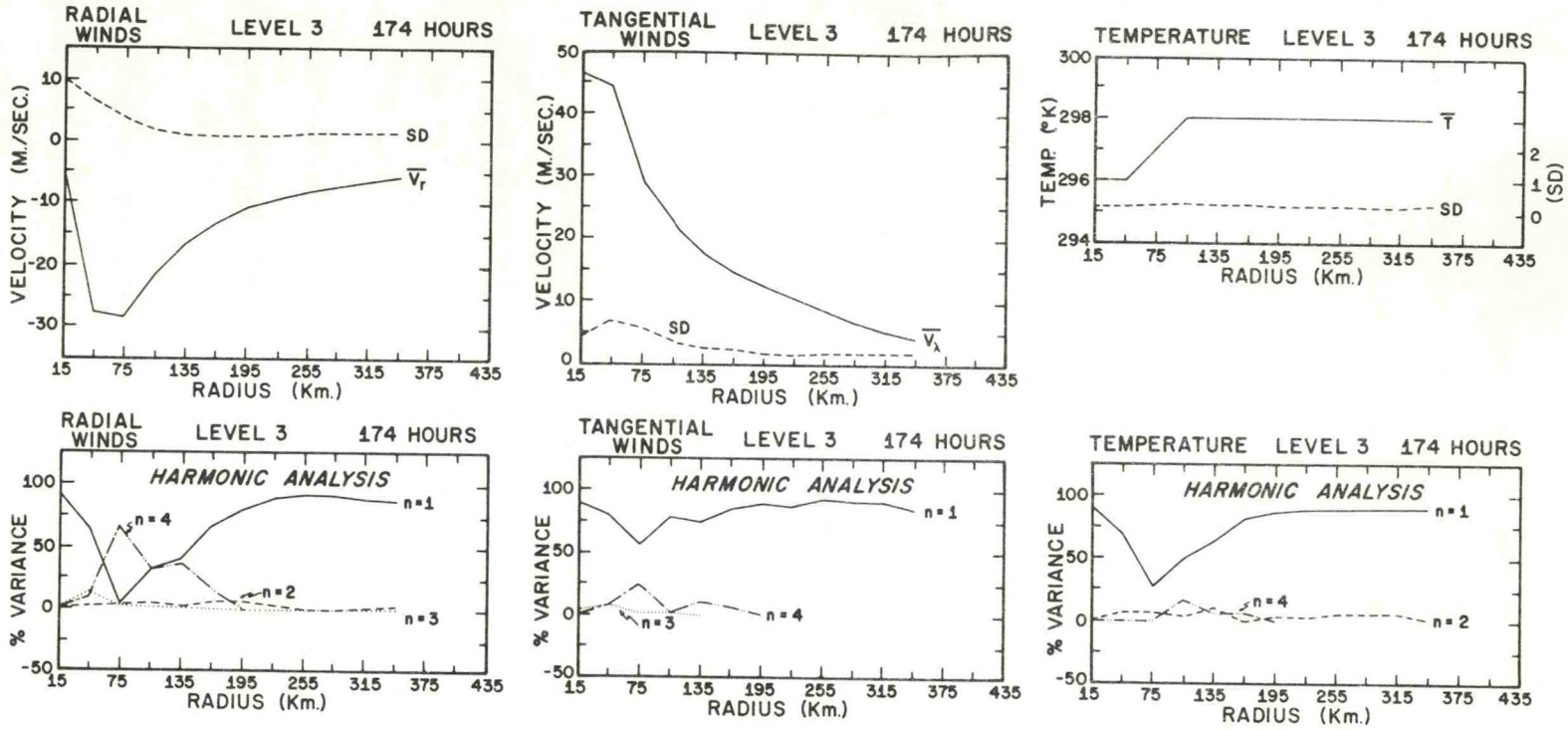

Figure 13: Standard deviations, azimuthal means, and harmonic analysis for the mature inflow layer.

This condition is probably artificial and is a manifestation of the initialization error due to the finite differencing scheme and boundary conditions. The standing wave number 4 does not occur in the upper outflow layer which is upstream from the lateral boundary.

The mean tangential wind component is characterized by a maximum cyclonic circulation of 47 m sec^{-1} at a radius of 15 km (fig. 13) which gradually diminishes to a value of 4 m sec^{-1} at R_{max}. For all radii, the SD remains small with a maximum of 7 m sec^{-1} at 45 km. The harmonic analysis shows that the greatest percent of the variance is contained in wave number 1. In summary, the small ratio of the SD to the mean indicates that the asymmetries in the boundary layer are much smaller than the asymmetries in the outflow layer.

The low-level temperature analysis (fig. 12) shows a maximum temperature deficit of 1.5°C. The deficit occurs at the vortex center with the remaining field characterized by flat gradients. Figure 13 displays the small SD found in the azimuthal mean temperatures and the strong boundary effects. Wave number 1 and 2 explain over 90% of the variance. Wave number 4 accounts for a smaller percent of the variance of temperature than of momentum.

6. HORIZONTAL TRANSPORT MECHANISMS

The time variations and the scale of the boundary and outflow layer asymmetries have been discussed in previous sections. This section investigates the importance of asymmetries as horizontal transport mechanisms. Computations of radially averaged horizontal and vertical fluxes of absolute vorticity and angular momentum are presented, with the greatest emphasis placed on the horizontal transports.

6.1 Flux of Absolute Vorticity

The mean and eddy transports of absolute vorticity, $\overline{v_r}^{\lambda}\,\overline{\zeta_a}^{\lambda}$ and $\overline{v_r'\,\zeta_a'}^{\lambda}$, for both the inflow and outflow levels of the model are presented in figure 14. The circularly averaged absolute vorticity, ζ_a, is given by

$$\overline{\zeta}^{\lambda} = \frac{\overline{\partial_r v_\lambda}^{\lambda}}{r\partial r} + f \qquad (7)$$

where f is the coriolis parameter. The operator $\overline{(\quad)}^{\lambda}$ refers to the azimuthal mean at a given radius and $(\quad)'$ refers to the departure from the mean. The outflow level flux of absolute vorticity shows that the eddy transports oppose the mean flux beyond 75 km. From 75 km to 165 km the eddy transport of vorticity is positive (outward) and dominant over the negative mean flux. Beyond 165 km, the mean flux becomes positive and is opposed by a negative eddy transport of vorticity of comparable magnitude. At the inner radii the mean and eddy transports are both positive with the mean flux much larger than the eddy flux.

The mean and eddy profiles of vorticity flux computed from the model experiment may be compared to similar profiles computed by Black and Anthes (1971) for real storms. Both model and real storms exhibit a radial annulus of substantial area in which the eddy transport of vorticity is negative and nearly balances the mean. This annular ring appears to be somewhat smaller in the model storm, a consequence perhaps of the overall small size of the model circulation. Comparisons near the center of the storm are difficult, because Black and Anthes' data begin at 111 km from the storm center, and the errors associated with their

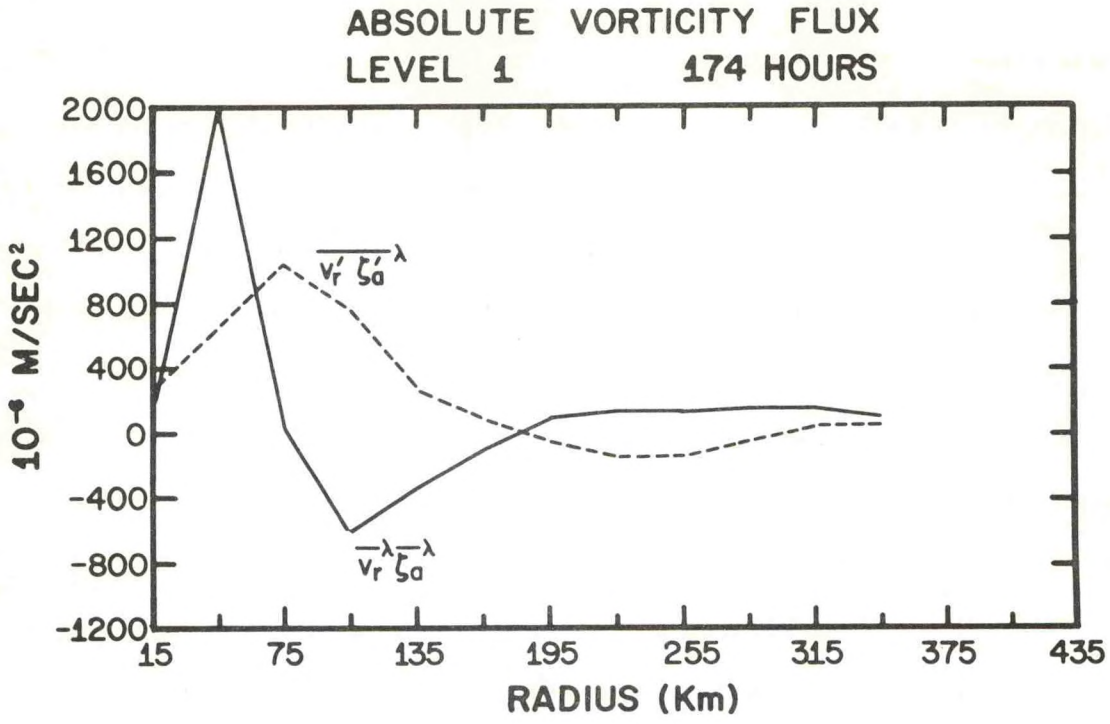

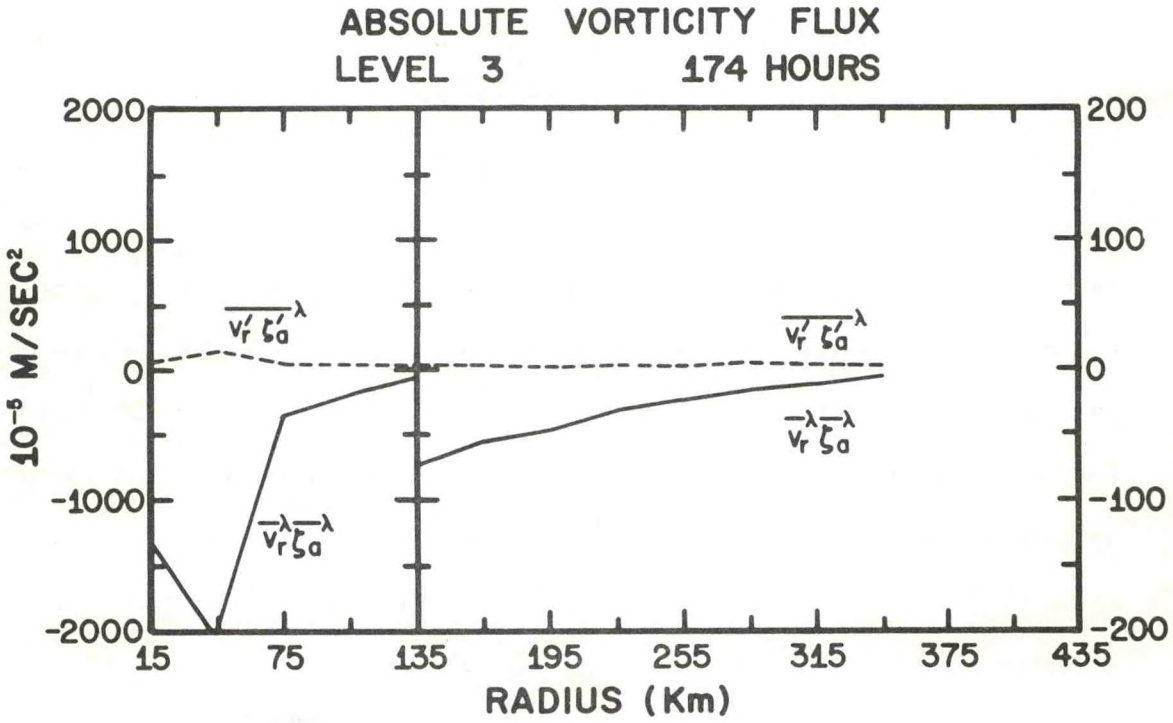

Figure 14: Profiles of mean and eddy transports of absolute vorticity for the model outflow and inflow levels.

measurements are maximum in this region. At the outer radii ($r \geq 195$ km) the model transports agree in sign and magnitude with observations.

In summary, the eddies in the outflow layer (at moderate distances from the storm center) convey absolute vorticity inward toward the storm center and oppose the outward vorticity flux by the mean flow in both the real and model storm.

The boundary layer flux of absolute vorticity (fig. 14) shows small positive eddy transports of vorticity at all radii in agreement with previous theoretical estimates (Anthes, 1970). The mean flux is strongly negative (inward) at all radii. Values range over two orders of magnitude. Therefore, vorticity is conveyed inward by the mean flow and completely dominates the eddy flow. This again emphasizes the basic symmetry in the inflow layer.

6.2 Flux of Angular Momentum

The mean, the eddy and the total transports of relative angular momentum, (weighted by radial distance), for both the outflow and inflow levels of the model are presented in figure 15. In the outflow layer, the mean flow transports negative momentum outward, while the eddies oppose the mean flow by transporting positive angular momentum outward. The mean and eddy terms are the same order of magnitude and tend to compensate for each other. In contrast, actual storm data of Black and Anthes (1971) show both components to have a net outward transport of negative relative angular momentum. However, the radial extent of the model is only half of that of the actual storm data and does not extend to the outer radii where the larger negative angular momentum fluxes are

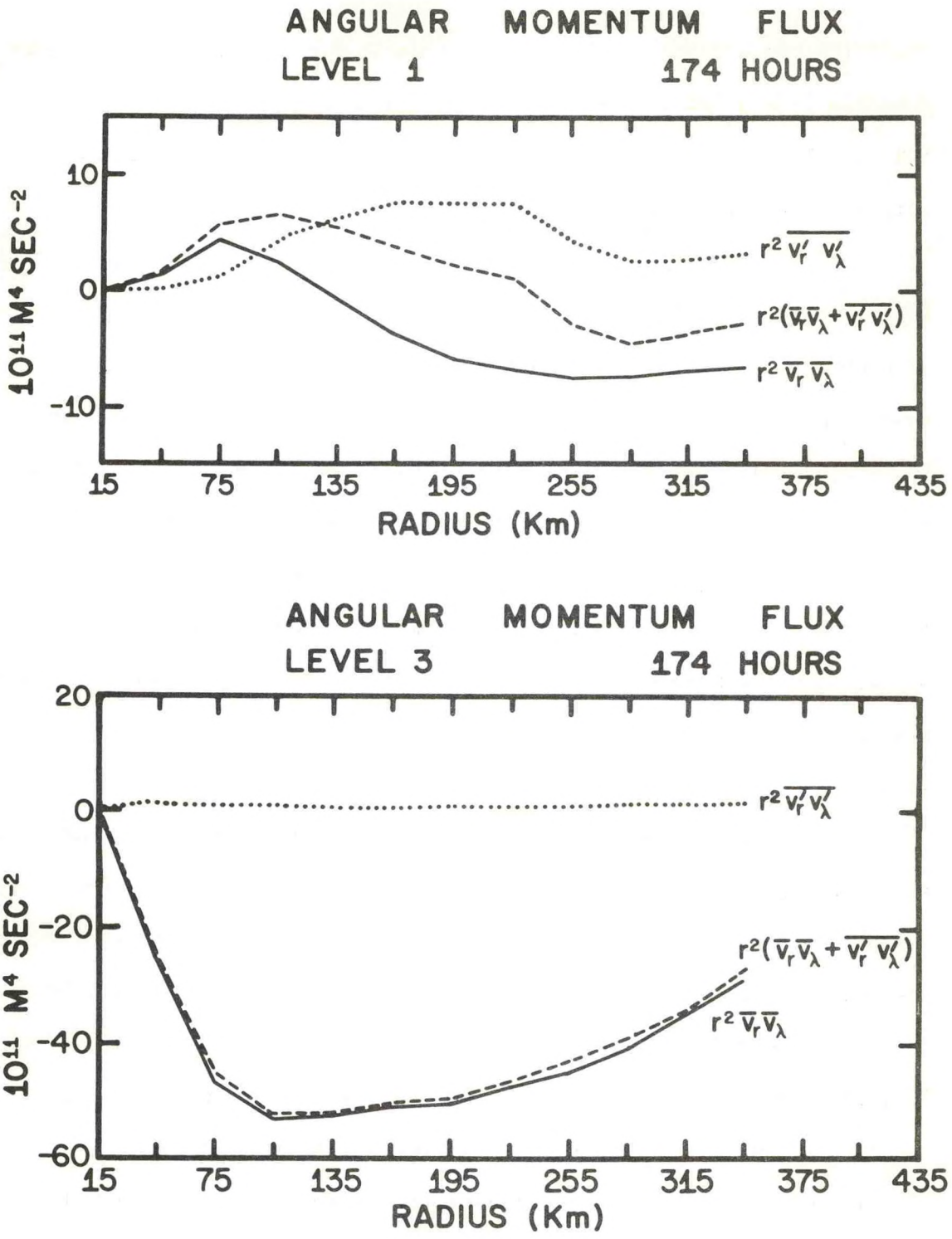

Figure 15: Profiles of mean ($r^2\overline{v}_r\overline{v}_\lambda$), eddy ($r^2\overline{v_r' v_\lambda'}$), and total ($r^2(\overline{v}_r\overline{v}_\lambda+\overline{v_r' v_\lambda'}$) transports of angular momentum for the model outflow and inflow levels.

found (Palmén and Riehl, 1957). In general, the magnitudes of the eddy momentum flux associated with the model and real storms are small inside 400 km. The model flux tends to be positive, and the flux associated with real storms tends to be negative.

The boundary layer flux of relative angular momentum (fig. 15) shows a very small outward eddy flux of positive angular momentum. The mean transport shows a strong inward flux of positive angular momentum. The mean completely dominates the eddy transport at all radii. This result is in agreement with Riehl and Malkus (1958), who found the eddy transports of momentum to be either negligible or outward in the inflow layer of hurricane Daisy. These results also agree with Pfeffer (1958) who found that within a few hundred kilometers from the vortex center the horizontal-eddy processes are of the wrong sign to account for the inward transport of angular momentum in the inflow layer of hurricane Connie, 1955.

In summary, the eddy transport of angular momentum in the model outflow layer is slightly positive; while in contrast, the eddy flux in real storms appears to be slightly negative. There is good agreement between the model and observations in the mean flux, however. In the inflow layer, the mean flux is dominant and is directed inward. The eddy flux is small, but directed outward, in good agreement with observations.

6.3 Vertical Flux of Relative Angular Momentum

It is of considerable importance to the overall dynamics of the model to determine the origin of the asymmetries in the outflow layer. As previously established, the outflow level is characterized by two

preferred quadrants of outflow (fig. 3). It is conceivable that azimuthal variation in the vertical flux of relative angular momentum could be responsible for the two streams of outflow.

Figure 16 shows azimuthal mean radial profiles of the mean vertical transport and eddy vertical transport of relative angular momentum, $(r \overline{v}_\lambda \overline{\dot{\sigma}}^\lambda)$, $(r \overline{v'_\lambda \dot{\sigma}'}^\lambda)$, where $\dot{\sigma}$ is the "vertical velocity" in the σ-system. The $\dot{\sigma}$ information levels are staggered in the vertical from the dynamic variables, necessitating the interpolation of the wind components to the $\dot{\sigma}$ levels. The radial profiles clearly show that the vertical flux of momentum is predominantly from the mean current. Although the outflow occurs in two quadrants the vertical motion is bringing momentum to the outflow level in a symmetric fashion. Thus the asymmetries are developing <u>after</u> the air reaches the outflow layer. This result is consistent with Anthes' (1972) findings that the asymmetries are a result of dynamic instability in the horizontal flow, with the eddies growing at the expense of the mean horizontal flow.

7. SUMMARY AND CONCLUSIONS

Conventional statistical techniques have been utilized to show the formation and structure of horizontal asymmetries in the outflow and inflow levels of a numerical hurricane model. The outflow layer is highly asymmetric, especially at the outer radii. The inflow layer contains relatively small asymmetries, and the approximation to axial symmetry is very good in the low levels. These results agree well with observations.

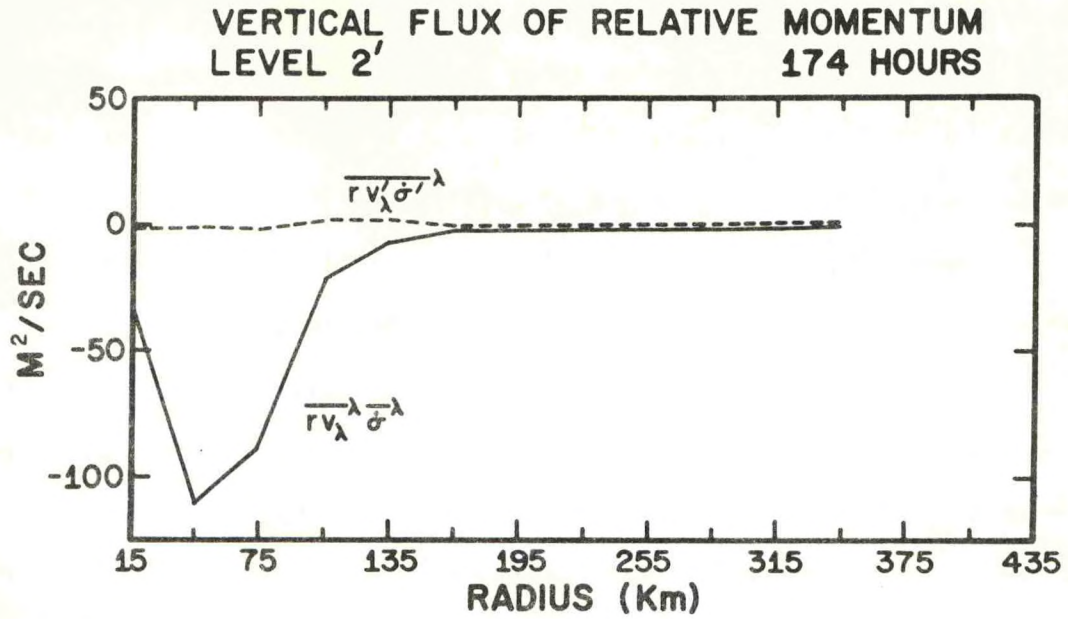

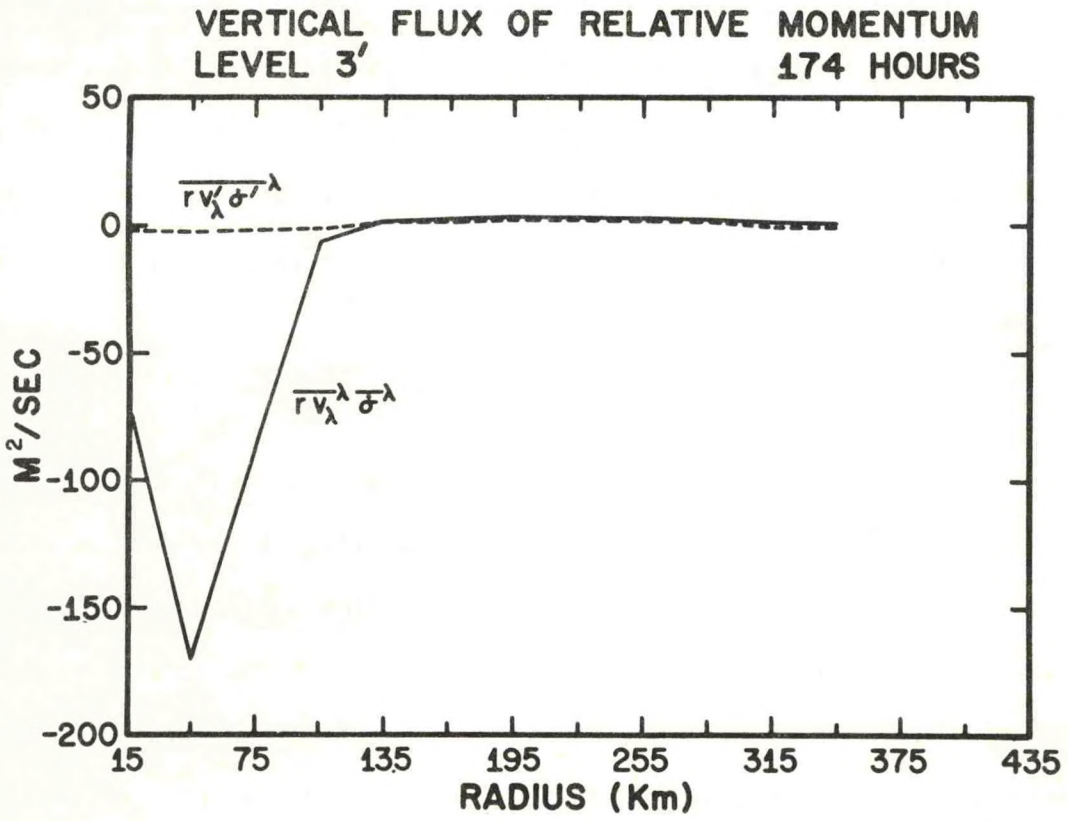

Figure 16: Profiles of mean and eddy vertical transports of relative momentum for the model outflow and inflow levels.

A comparison with real storms reveals that the model is capable of reproducing many observed features of the mature three-dimensional tropical cyclone. Slight differences between the observed and model vortices are attributed to the limited lateral extent of the model as the errors associated with the irregular boundary.

The mean transport of absolute vorticity beyond 200 km in the outflow layer is outward from the storm center and is opposed by the eddy flux of absolute vorticity in both the real and model vortices. The mean flux of absolute vorticity in the model inflow layer is strongly inward and completely dominates the small eddy flow, in agreement with real storms. Beyond 135 km, the mean transport of relative angular momentum in the outflow layer is negative; the eddy flux of angular momentum is positive. Radial profiles of the vertical flux of momentum show that the vertical transport of momentum is dominated by the mean current, indicating that vertical eddies play no important role in the formation of the eddies in the outflow layer.

8. REFERENCES

Anthes, R. A. (1972), The development of asymmetries in a three-dimensional numerical model of a tropical cyclone, Monthly Weather Review, (in press).

Anthes, R. A. (1970), The role of large-scale asymmetries and internal mixing in computing meridional circulations associated with the steady-state hurricane, Monthly Weather Review, 98, No. 7, July, 521-528.

Anthes, R. A., S. L. Rosenthal, and J. W. Trout (1971a), Preliminary results from an asymmetric model of the tropical cyclone, Monthly Weather Review, (in press).

Anthes, R. A., J. W. Trout, and S. S. Ostlund (1971b), Three dimensional particle trajectories in a model hurricane, Weatherwise, (in press).

Anthes, R. A., J. W. Trout, and S. L. Rosenthal (1971c), Comparisons of tropical cyclone simulations with and without the assumption of circular symmetry, Monthly Weather Review, (in press).

Black, P. G. and R. A. Anthes (1971), On the asymmetric structure of the tropical cyclone outflow layer, Journal of the Atmospheric Sciences, (in press).

Black, P. G. (1971), Use of echo velocities to evaluate hurricane modification experiments, Project STORMFURY Annual Report 1970, U. S. Department of the Navy and U. S. Department of Commerce, Appendix J, J-1 - J-20.

Gray, W. M. (1967), The mutual variation of wind, shear and baroclinicity in the cumulus convective atmosphere of the hurricane, Monthly Weather Review, 95, No. 2, February, 55-73.

Izawa, T. (1964), On the mean wind structure of typhoons, Typhoon Research Laboratory, Technical Note N . 2, Meteorological Research Institute, Tokyo, Japan.

Koss, W. J. (1971), Numerical integration experiments with variable resolution two-dimensional cartesian grids using the box method, Monthly Weather Review, (in press).

Kurihara, Y. and J. L. Holloway (1967), Numerical integrations of a nine-level global primitive equation model formulated by the box method, Monthly Weather Review, 95, No. 8, August, 509-530.

Matsuno, T. (1966), Numerical integrations of the primitive equations by a simulated backward difference method, Journal of the Meteorological Society of Japan, 44, February, 76-83.

Miller, B. I. (1958), The three-dimensional wind structure around a tropical cyclone, National Hurricane Research Project Report 15, U. S. Department of Commerce, National Hurricane Research Laboratory, Miami, Florida, January, 41 pp.

Palmén, E. and H. Riehl (1957), Budget of angular momentum and energy in tropical cyclones, Journal of Meteorology, 14, 150-159.

Pfeffer, R. L. (1958), Concerning the mechanics of hurricanes, Journal of Meteorology, 15, 113-119.

Phillips, N. A. (1957), A coordinate system having some special advantages for numerical forecasting, Journal of Meteorology, 14, April, 184-185.

Riehl, H. and J. S. Malkus (1958), Some aspects of hurricane Daisy, Tellus, 13, 181-213.

Rosenthal, S. L. (1971), A circularly symmetric primitive equation model of tropical cyclones and its response to artificial enhancement of the convective heating functions, Monthly Weather Review, 99, No. 5, May, 414-426.

Rosenthal, S. L. (1970a), Experiments with a numerical model of tropical cyclone development--some effects of radial resolution, Monthly Weather Review, 98, No. 2, February, 106-120.

Rosenthal, S. L. (1970b), A circularly symmetric primitive equation model of tropical cyclone development containing an explicit water vapor cycle, Monthly Weather Review, 98, Vol. 9, September, 643-663.

Rosenthal, S. L. (1969), Numerical experiments with a multilevel primitive equation model designed to simulate the development of tropical cyclones: experiment I, ESSA Technical Memorandum ERLTM-NHRL 82, U. S. Department of Commerce, National Hurricane Research Laboratory, Miami, Florida, 36 pp.

Smagorinsky, J., S. Manage, and J. L. Holloway (1965), Numerical results from a nine-level general circulation model of the atmosphere, Monthly Weather Review, 93, No. 12, December, 727-768.